International Journal of Researches on Civil Engineering with Artificial Intelligence

www.ceai.reapress.com

Int. J. Res. Civ. Eng. AI. Vol. 1, No. 1 (2024) 1–20.

Paper Type: Original Article

Enhancing Shear Strength in Retrofitted Reinforced Concrete Beams with Fiber-Reinforced Polymers: An Artificial Neural Network Approach

Simon James[1], Tiana T Thiagi[2,*]

[1] Department of Civil Engineering, Faculty of Engineering, Universiti Malaya, 50603, Kuala Lumpur, Malaysia; sgj@deakin.edu.au;
[2] Taylor's University Lakeside Campus, Petaling Jaya, No.1 Jalan Taylor's, 47500 Subang Jaya, Selangor, Malaysia; tianatthiagi1@outlook.com

Citation:

Received: 14 February 2024 *Revised: 17 March 2024* *Accepted: 07 April 2024*	James, S., & Thiagi, T. T. (2024). Enhancing shear strength in retrofitted reinforced concrete beams with fiber-reinforced polymers: an artificial neural network approach. *International journal of researches on civil engineering with artificial intelligence*, *1*(1), 1-20.

Abstract

Fiber-Reinforced Polymers (FRP) have attracted much attention as a promising solution for preserving existing Reinforced Concrete (RC) buildings. Structures could be maintained by reinforcing, repairing, or retrofitting to address seismic inadequacies. For RC beams, shear failure is identified as the most catastrophic failure mode due to the lack of failure warning. However, there is not enough information on the shear behavior of these retrofitted beams, especially regarding the ideal design and placement of the FRP composites. This study aims to examine the shear strength of RC beams retrofitted with FRP composites and identifies the most efficient design and deployment procedures for these composites. The Artificial Neural Network (ANN) algorithm enhances the precision and efficiency of forecasting the shear strength, increases the solidity and durability of RC structures, and reduces the need for expensive repairs or replacements. Three RC beams were examined experimentally under combined torsion and shear. ANN values of RMSE = 0.466, R^2 = 0.856, and r = 0.945 indicate a satisfactory correlation between experimental and numerical values and the AI model's reliability. The results of each training set are near 1 when considering the R^2 values, regardless of torsion or shear exposure of the retrofitted T-beams. The test set R^2 values of A1, A2, and AB under torsion and shear demonstrate correct ANN performance. Fiber reinforcement and the volumetric ratio of the FRP materials determine the final structural strength of RC beams enhanced with FRP. Higher torsional reinforced beams have a larger torsional capacity, final angle of twist, and enhanced post-cracking rigidity for a given twist angle.

Keywords: Shear strength, RC beams, Retrofitted FRP composites, Artificial neural network, Nonlinear behavior, RC structures, Fiber-reinforced polymers.

1 | Introduction

RC thin beams often fail due to brittle shear, a severe type of failure. A RC slender beam is a sort of RC structural element having a high shear span-to-height rate (a/h) or span-to-depth rate (a/d) or other values

Corresponding Author: sgj@deakin.edu.au;

are described in distinct works, such as (a/d) > 2.5 in Kani [1] and ACI 318 [2], (a/d) > 2 in JSCE, and (a/h) > 3 in EC2 [3]. The shear behavior of RC slender beams is affected by some parameters such as concrete Compressive Strength (CS), shear span-to-depth ratio, stirrup ratio, and longitudinal reinforcement ratio are some parameters [4]–[7]. There has been a great investigation into the shear performances of RC slender beams, and several shear models have been presented. Engineers must have a shear strength model that can accurately anticipate results in the real world [8]–[13]. According to the processes and techniques, the current shear strength formulae of RC beams may be classified into five broad categories: mechanics-based approaches, empirical Machine Learning (ML)-based models, semi-empirical models, and probabilistic models. Empirical models include the most important influencing factors and are created solely through regression analysis of experimental data. The semi-empirical models are built following the mechanical-based models, and their factors are derived by fitting the results of shear tests. The shear models in the ACI318 [2] and GB50010 standards are semi-empirical and currently used to derive shear strength formulae in international codes. *Fig. 1* shows the mixture process of concrete, including cement, aggregates, and fibers.

Fig. 1. Mix processing of cement, aggregates, and fibers.

Many researchers have worked on steel-RC members, specifically their shear behavior, for over a century [9], [13]–[18]. Despite various problems with shear behavior and characterization of the complex shear resistance operation of RC members, there is still a lack of understanding of the operation and behavior of shear resistance. Fiber-Reinforced Polymers-Reinforced Concrete (FRP-RC) members behave differently in shear than steel RC members because of their unique mechanical characteristics [19]. Many questions remain to be answered about the sheer concerns of FRP-RC members that are up for debate. Previous research [20]–[22] also shows that the current shear design formulas are quite cautious when estimating the shear capacity of FRP-RC beams. As a result, additional FRP utilized to prevent shear may be expensive and lead to reinforcement density. The shear strength of RC beams with no web reinforcement was remarked to change depending on different criteria, including the concrete strength (f_c'), beam depth (d), shear span-to-depth ratio (a/d), beam width (b_w) and longitudinal reinforcement ratio (ρ_f) [23], [24]. The type of FRP rebar used and its unstable mechanical characteristics, such as low elastic modulus (E_f), low transverse shear strength and high Tensile Strength (TS) must also be considered when designing FRP-RC components. Even though several investigations have been undertaken to estimate the shear strength of FRP-RC parts in both theoretical and practical scenarios and to examine the interplay of major factors in shear strength processes, there is no consensus on a particular model at this time. The great majority of current shear design formulas have diverse types and do not provide a proper factor against shear failure [25]–[27]. In addition, no consensus happened among current codes and equations about the factors influencing shear capacity. This debate in prediction models may be linked to two primary causes: first, the lack of an understanding theory on shear failure owing to its complex behavior and rapid and catastrophic failure type, and second, the broad variation in the mechanical characteristics of FRP bars. Also, as another choice to traditional and typical methodologies,

Artificial Intelligence (AI) algorithms such as Artificial Neural Networks (ANN), Fuzzy Inference Systems (FIS), and Genetic Programming (GP) may forecast complex challenges in many various areas in the shear strength of FRP-RC members [28]–[31]. These approaches have been widely used and highly successful in many scientific usages, especially in civil engineering, over the past two decades. The shear capacity of FRP-RC elements in the absence of stirrups has recently been predicted using various AI methods. Using Gene Expression Programming (GEP) by Kara [32] yielded a basic model from 104 databases. Bashir and Ashour proposed a model based on ANN [33] using 128 data sources. Using a 128-model database, Nasrollahzadeh and Basiri [34] created a FIS. To propose their theoretical model using ANN, Lee and Lee [35] compiled a dataset of 110 instances. On the back of 138 experimental specimens and a novel method of biogeography-based programming, Golafshani and Ashour [36] presented a method. While this research generally proposed accurate models, their database sizes were limited. Model performance is highly dependent on the database size for training and testing. *Fig. 2* shows the shear failure test.

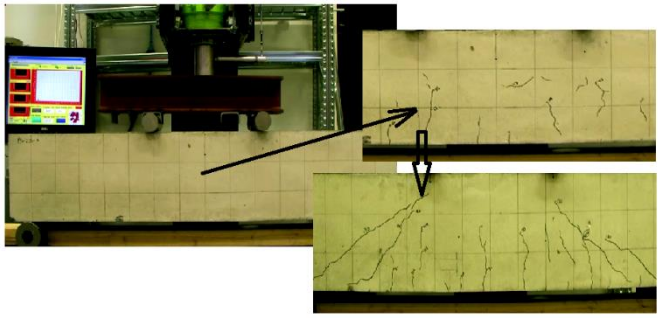

Fig. 2. Shear test in FRP-RC: the first crack was seen at 60.1 KN, shear failure at 70.2 KN, and breaking time at 32.6 min.

Full-Wrap (FW), U-Wrap (UW), and Side Bond (SB) are three famous methods for external shear reinforcement of RC components. In the first method, FW, the FRP completely encircles the section. The FW scheme is the most efficient of the three common fortification methods. In UW, the FRP composites are fastened to the beams' bottom, middle, and top faces (but not the top), while in SB, they're just fastened to the RC beams' side faces. In the case of RC beams or columns, it can be used on any of the four sides if they are rectangular. Slab-girder buildings frequently employ lateral bonding or U-wrapping to get around these issues. However, the UW configuration outperforms the SB scheme [37]. In shear, slab-on-beam structures, like those used in RC T-beam experimental studies [38], [39], are more stable than rectangular RC beams. Generally, the structural design prioritizes bending moments and shear forces over torsion. However, in cases where spandrels or curved beams are present, the effect of torsion becomes more noticeable. Experiments in the past have mostly focused on EB-FRP-strengthened RC rectangular or box beams subjected to monotonic torsion [40]–[44]. Compound loads, including torsion and bending, or torsion and shear, are placed on many structural elements. Some research has examined the behavior of retrofitted RC T-beams subjected to shear, pure, and combined torsion [45], [46].

Effective strain prediction was provided by some models in [38], [39], and [45] based on FIB [47], which primarily used shear testing rather than torsional tests [48]. However, compiling a thorough dataset of empirical research on RC T-beams strengthened with EB-FRP and exposed to torsion and shear in tandem is essential. However, a finite element (FE) analysis utilizing commercial applications is a useful addition to studying the structural action of retrofitted RC beams because experimental work is costly and time-consuming. RC beam torque-torsional curves and the impact of FRPs on structural behavior have been studied numerically, applying FE software such as ANSYS, Algor SAP, ABAQUS, DIANA, etc. [40]. Bernardo et al.'s studies [49] on the Generalized Softened Angle Truss Model (GSVATM) examined how RC beams responded to torsion and axial forces combined. Their theoretical forecast on (MT− θ) was consistent with their FE models of reference beams. Protchenko et al. [50] investigated how high temperatures affected the structural capabilities of RC elements that had internal FRP reinforcements. Carbon fibers' high thermal expansion coefficient causes FRP bars to creep, which results in the pre-stressing property of beams. In this

instance, they saw that the deviation started to reduce after a particular temperature threshold. Salih et al. examined the impact of FRP on the cyclic action of RC beams with apertures [51]. Their experimental findings demonstrated the FRP sheets' significant impact on enhancing the structural capabilities of their RC beam instances. They also considered parametric research on bond length and opening size conducted by ABAQUS. The experiments and the FE analysis showed that the square columns with the FRP retrofits had increased strength and stiffness under compression. The impact of FRP and Textile-Reinforced Mortars (TRM) in improving the structural capabilities of retrofitted RC T-beams was shown by Pohoryles et al. [52] in their empirical FE study. In recent years, there has been a remarkable advancement in the development of many engineering research studies using AI and neural networks. Abdolrasol et al. [53] performed in-depth research on ANN applications and real-world optimization methods such as Backtracking Search Algorithm (BSA), Whale Optimization Algorithm (WOA), Particle Swarm Optimization (PSO), Lightning Search Algorithm (LSA), Genetic Algorithm (GA), and Artificial Bee Colony (ABC).

The technical results of his study showed the application of AI models to improve the ANN's efficiency. Several important parameters, including material geometry, strength, stain, confinement, and FRP properties, were incorporated into three ML methods for FRP strain forecast, presented by Abdalrhman Milad et al. [54]. FRP composite strain enhancement ratios could be predicted using five different input combinations based on these parameters. Several different computer-assisted methods for designing engineering strain-based challenges were proposed, including Multivariate Adaptive Regression Spline (MARS), Extreme Gradient Boosting (XGBoost), and Random Forest (RF). The shear strength of RC beams was predicted by applying (ANN), Multi-Layer Perceptrons (MLP), and Adaptive Neuro-Fuzzy Inference Systems (ANFIS) by Amani and Moeini [55]. They compared their findings to standards the American Concrete Institute (ACI) and the Iranian Concrete Institute (ICI) set forth. As a result of their analysis, they proved the usefulness of ANN programs for forecasting structural behavior.

1.1 | Problem Statement

The problem statement of this study is to investigate the shear strength of RC beams that have been retrofitted with Fiber-Reinforced Polymer (FRP) composites and to determine the most effective design and placement methods for these composites. Shear failure is identified as the most disastrous failure mode for RC beams, as it does not give any warning before failure. Using ANN can potentially improve the accuracy and efficiency of predicting the shear strength compared to traditional methods, ultimately improving the strength and durability of RC structures and reducing the need for costly repairs or replacements. The study aims to use four RC beams that will be experimentally investigated under combined torsion and shear. *Fig. 3* shows two models of fibers in concrete mixture: when fibers are randomly distributed, they provide a homogenous distribution throughout the concrete, which can improve its overall strength and toughness. On the other hand, when fibers are aligned, they are oriented in a specific direction to provide enhanced properties in that direction. This can be useful in applications with a specific strength direction, such as pre-stressed concrete beams.

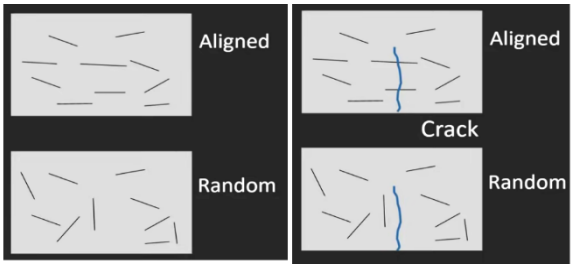

Fig. 3. Two models of fiber distribution in concrete mixture: random, aligned.

1.2 | Significance of Study

The significance of this study lies in its ability to improve the comprehension of the shear behavior of RC beams retrofitted with FRP composites. By investigating the shear strength of these beams and determining the most effective design and placement methods for the FRP composites, this research aims to improve the overall solidity and durability of RC buildings, potentially reducing the need for costly repairs or replacements. Additionally, the use of ANN in this study has the potential to increase the precision and efficiency of predicting the shear strength compared to traditional methods. This is important since ANN can model a wide range of complex and nonlinear behaviors, which can be difficult to achieve with traditional analytical methods. Furthermore, this research aims to analyze the effect of torsion on the shear strength of the beams, which can lead to a more accurate forecast of the shear strength for retrofitted RC beams under various loading conditions and help to understand the behavior of the beams under the combination of torsion and shear. Overall, the findings of this research can contribute to the development of more beneficial and efficient design methods for retrofitting RC structures with FRP composites, which will ultimately help to improve the safety and longevity of these structures. The final structural strength of FRP-reinforced RC T-beams is determined by the volumetric ratio and fiber orientation of the FRP materials utilized (*Fig. 4*).

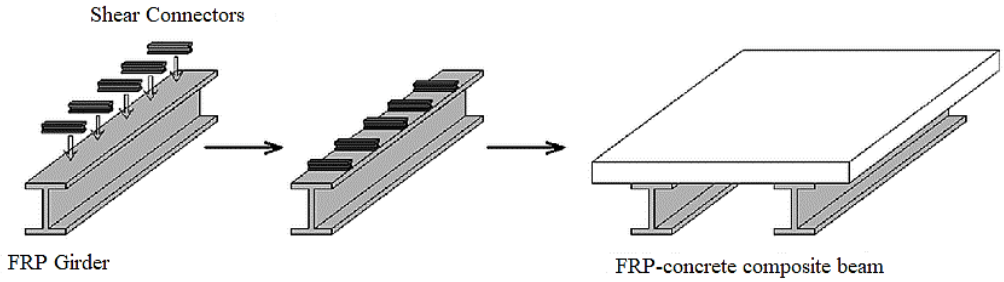

Fig. 4. Typical FRP-concrete composite beam, reproduced from [56].

2 | Methodology

2.1 | Materials

The concrete mix proportion utilized in RC beams for proper depths is 180 mm × 400 mm. To manage volumetric variations in concrete, three mix proportions were formulated. All the concrete samples employed the same water-to-binder ratio (W/B) and the same volumetric rate for the liquid (water plus the Shrinkage-Reducing Agent (SRA)) and aggregate contents. The amounts and ratios of the materials used in the study are Cement: 3.16 g/m^2, Water: 300, Water-to-cement ratio (w/b): 60%, Lime stone: 3.50 cm^2/g, Fine aggregate: 2.70 g/m^3, High shrinkage coarse aggregate: 2.60 g/m^3, Normal coarse aggregate: 2.50 g/m^3. Table 1 lists the mechanical characteristics of concrete and steel bars: CS, TS, Elastic Modulus E_c for concrete and Elastic Modulus E_s, Yield Strength σ_{ts}, and Ultimate Strength for steel bar. *Table 2* displays the material properties of FRP. Based on the information provided, the methodology for testing the shear strength of the RC beams A1, A2, and AB would involve the following steps:

I. Prepare the concrete mixture: mix the cement, water, limestone, fine aggregate, high shrinkage coarse aggregate, and normal coarse aggregate in the specified proportions to form the concrete mixture.

II. Cast the beams: use formwork to shape and hold the concrete in place while it cures. The beams should be cast with the specified dimensions of height (AB (control) with 100mm, 200 mm for A1, and 600 mm for A2) and width (200 mm for A1, A2, and AB), and effective depth (1000 for AB, 1500 mm for A1 and 4500 mm for A2).

III. Cure the beams: allow them to cure for a specified period, typically at least 7 days, to ensure the concrete reaches its full strength.

IV. Apply the load: apply the nominal load for shear failure (130 KN for AB, 134 KN for A1, and 280 KN for A2) and the nominal load for bending failure (300 KN for AB, 340 KN for A1, and 1000 KN for A2) to the beams using a loading frame or similar device.

V. Measure the deflection: measure the deflection of the beams under load using a displacement transducer or similar device.

VI. Result analysis: calculate the beam's shear strength by dividing the nominal load for shear failure by the total area of the beam. Analyze the results to determine the most effective design and placement methods for the FRP composites and investigate torsion's impact on the beams' shear solidity.

VII. Results comparison: compare the findings with the existing analytical methods and the forecast of the shear strength using ANN.

Table 1. Mechanical parameters of concrete and steel bar.

Concrete		Steel Bar			
TS σ_{tcmax}	CS σ_{ccmax}	EM E_c	EM E_s	YS σ_{ts}	US
2.4MPa	28.1MPa	31GPa	198GPa	331MPa	453MPa

Table 2. Material properties of FRP.

T mm	FA(mm²)	UL/N	S MPa	ME GPa	FS
1	1.83	4032	2143	92.45	2.34%

Thickness=T, Fiber Area=FA, Ultimate Load=UL, Strength= S, Modulus of Elasticity= ME, Fracture Strain=FS.

2.2 | Equation Design

Eqs. (1)-(11) present the existing Equation for V_{cf}. Because these equations were empirically derived, there is a significant gap between identifying the primary parameters and their impact on V_{cf}. There are some parameters in the next equations as follows: E_c, E_s and E_f = moduli of elasticity for concrete, d = member effective depth; steel, b_w = member web width; and FRP, respectively; f_{cu} = cube CS of concrete; $n = E_f/E_c$; β_1 = flexural rectangular compressive stress block parameter; and ρ_f = flexural FRP reinforcement ratio.

ACI Committee 440 [57]

$$V_{cf} = \frac{\rho_f - E_f}{90\beta_1 f_c'}\left(\frac{\sqrt{f_c'}b_w d}{6}\right). \quad (1)$$

ACl440.1R-06

$$V_{cf} = \frac{2}{5}k_n\sqrt{f_c'}b_w d, \quad (2)$$

where $k_n = \sqrt{2\rho_f n + (\rho_f n)^2} - \rho_f n$.

BISE design guidelines [58]

$$V_{cf} = 0.79\left(100\rho_f\frac{E_f}{E_s}\right)^{1/3}\left(\frac{400}{d}\right)^{1/4}\left(\frac{f_{cu}}{25}\right)^{1/3} b_w d. \quad (3)$$

CSA S806-2

$$\text{For } d \leqslant 300 \text{ mm: } V_{cf} = 0.035\lambda\phi_c\left(f_c'\rho_f E_f\frac{V_f}{M_f}d\right)^{\frac{1}{3}} b_w d \quad (4a)$$

$$0.1\lambda\phi_c\sqrt{f'_c}b_w d \leqslant V_f \leqslant 0.2\lambda\phi_c\sqrt{f'_c}b_w d.$$

For

$$d > 300 \text{ mm: } V_{ff} = \left(\frac{130}{1000+d}\right)\lambda\phi_c\sqrt{f'_c}b_w d \geqslant 0.08\lambda\phi_c\sqrt{f'_c}b_w d\frac{V_f}{M_f}d \leqslant 1.0. \quad \textbf{(4b)}$$

($\lambda = 1.0$ and $\phi_c = 1.0$ for this research).

ISIS-M03-01 [59]

$$\text{For } d \leqslant 300 \text{ mm: } V_{cf} = 0.2\lambda\phi_c \cdot \sqrt{f'_c}b_w d\sqrt{\frac{E_f}{E_s}}. \quad \textbf{(5a)}$$

Or

$$\begin{aligned} d > 300 \text{ mm: } V_{cf} &= \left[\frac{260}{1{,}000+d}\right]\lambda\phi_c \cdot \sqrt{f'_c}b_w d\sqrt{\frac{E_f}{E_s}} \\ &\geqslant 0.1\lambda\phi_c\sqrt{f'_c} \cdot b_w d\sqrt{\frac{E_f}{E_s}}. \end{aligned} \quad \textbf{(5b)}$$

JSCE shear design method [60]

$$V_{cf} = \frac{\beta_d\beta_\rho\beta_n f_{icd}b_w d}{\gamma_b}, \quad \textbf{(6)}$$

where

$$V_{cf} = \beta_d\beta_\rho\beta_n f_{zcd}b_w d/\gamma_b,$$
$$f_{bed} = 0.2(f'_c)^{(1/3)} \leqslant 0.72,$$
$$\beta_d = \left(\frac{1000}{d}\right)^{(1/4)} \leqslant 1.5,$$
$$\beta_\rho = \left(100\rho_f\frac{E_f}{E_s}\right)^{(1/3)} \leqslant 1.5,$$
$$\beta_n = \begin{cases} 1+\dfrac{M_c}{M_d} \leqslant 2 \text{ for the } N'_d \geqslant 0, \\ 1+\dfrac{M_o}{M_d} \geqslant 0 \text{ for the } N'_d < 0, \end{cases}$$
$$\gamma_b = 1.0 \text{ for the current day.}$$

Michaluk et al. [61]

$$V_{cf} = \frac{E_f}{E_s}\left(\frac{1}{6}\sqrt{f'_c}b_w d\right). \quad \textbf{(7)}$$

Deitz et al. [62]

$$V_{cf} = 3\frac{E_f}{E_s}\left(\frac{1}{6}\sqrt{f'_c}b_w d\right). \quad \textbf{(8)}$$

Tureyen and Frosch [63]

$$V_{cf} = \frac{5}{12}k_n\sqrt{f'_c}b_w d. \quad \textbf{(9)}$$

El-Sayed et al. [64]

$$V_{cf} = \left(\frac{\rho_f E_f}{90\beta_1 f_c'}\right)^{1/3}\left(\frac{\sqrt{f_c'}}{6} b_w d\right) \leqslant \frac{\sqrt{f_c'}}{6} b_w d. \quad (10)$$

Razaqpur and Isgor [21]

$$V_{cf} = 0.035 k_m k_s k_a (1 + k_r)\sqrt{f_c'} b_w d \leqslant 0.2 k_s \sqrt{f_c'} b_w d, \quad (11)$$

where

$$k_m = \left(\frac{V_F d}{M_F}\right)^{2/3},$$

$$k_r = (E_f \rho_f)^{1/3},$$

$$k_a = \begin{cases} 1.0, & \text{for } \left(\frac{M_f}{V_f d}\right) \geqslant 2.5, \\ \frac{2.5}{(M_f/V_f d)}, & \text{for } \left(\frac{M_f}{V_f d}\right) < 2.5, \end{cases}$$

$$k_s = \begin{cases} 1.0, & \text{for } d \leqslant 300 \text{ mm}, \\ \frac{750}{450 + d}, & \text{for } d > 300 \text{ mm}. \end{cases}$$

2.3 | ANN Development

ANNs are mathematical representations of the human neural system. Several decades ago, researchers began developing these models to make them more human-like in areas such as pattern recognition and classification. Due to the availability of ever more powerful computing devices, ANNs are being used in areas such as decision-making and prediction that formerly required the involvement of human experts. In general, ANNs consist of several layers, each consisting of several nodes called neurons. All of the layer's neurons are directly linked to all the neurons in the above layer. For each connection, a weighting factor is assigned. This factor weights each neuron's output to the next layer's neuron. As the status of each neuron, the sum of all the weighted inputs to this neuron, plus a constant weight assigned to each neuron, is defined. This constant weight is called "Threshold" or "Bias Term". The output of each neuron is a function of its status. The name of this function is "Activation Function". The neuron's activation function may be either a linear or a nonlinear function of the status. Selecting a particular activation function depends on the problem the neuron is trying to solve. As a first step in defining this architecture, two ANNs should be developed, one that would connect the physical/engineering parameters to the psycho-acoustic parameters and the other that would connect the psycho-acoustic parameters to the Comfort Index.

Furthermore, it was decided that two different ANNs should be developed depending on the type of aircraft that they would be implemented on, one for airplanes and another for helicopters. After extensive research and testing, it was decided that the ANN scheme described above would have the following architecture and parameters: ANN 1: The first part of the ANN scheme consists of a Radial Basis Network. The input vector of the network has 560 values, representing 35 spectra, each having 16 dB values, for 16 frequency ranges or corresponding third-octave values (a frequency range related to vibrations was not included) [65].

3 | Discussion

3.1 | FRP Effective Strain Equation Development

The available empirical information is first used to define the proper FRP strain experimentally. The elastic modulus, area of FRP fibers, and concrete strength are then used to construct the power-type formula. The same calculation is then used to calculate the shear strength of the FRP-enhanced joints and compare it with

the shear strength of the joints as measured in an experiment. This section provides a quick summary of the process. By using the empirical information, the formula for Effective FRP strain is given as follows:

$$\varepsilon_{f,}^{cxp} = \frac{P_{i_f f}^{exp} \cdot b_c - h_e}{A_{f,q} \cdot E_f \cdot \sin\ \theta}. \quad (12)$$

As measured experimentally, the portion of FRP to the primary tensile stress $\left(p_{t,f}^{exp}\right)$ is given by

$$p_{t,f}^{exp} = \left(p_{t,tot}^{Exp}\right) - (p_{ct}), \quad (13)$$

where $p_{t,}^{exp}$ represents the major tensile stress of the reinforced FRP beam to the column junction and $p_{c,t}$ displays an enhancement in the primary tensile stress of the joint panel caused by concrete. The following Equation is used to calculate the total primary tensile stress $\left(p_t = p_{t,\,tot}^{exp}\right)$ using the Mohr's circle method

$$p_{t,itt} = \frac{-\sigma_c}{2} \cdot \sqrt{\left(\frac{\sigma_c}{2}\right)^2 + \nabla_{j\,h}\,^2}. \quad (14)$$

The interior BCJ of a deformed bar is used to calculate the concrete's contribution to the tensile stress.

$$p_{l,c} = k \cdot \sqrt{f_c}. \quad (15)$$

The numeric ratio k is taken as 0.29 when using deformed bars (during the initial breaking of the joint) and 0.42 otherwise (at peak strength). Maximum joint breakage and peak strength for a smooth internal reinforcement are both derived at $k = 0.20$ [66]. Priestley [67] is the only two examples of authors who have advocated for constraints on compression principal stresses (p_c) likewise, average tensile principal stresses are ppresens in tension in tension. According to their experiments, the compression primary stresses (p_c) need to be limited to levels proportional to the CS of concrete, as shown in *Eq. (16)*.

$$p_c = \frac{\sigma_c}{2} \cdot \sqrt{\left(\frac{\sigma_c}{2}\right)^2 + \sigma_{j\,h^2}} \le 0.5 f_c\,. \quad (16)$$

Remark: In some studies, $p_{1,\,tot}^{exp}$ is shown by f_1. Likewise, σ_c [68] is shown by f_a [69] in some studies. $\sigma_c = F_a$ = axial compressive stress = (axial force)/(joint x-area). The attention was turned out to find compressive stress's direction, θ. Here, the equations presented by [46] (also applied by [68], [69]) were used as follows:

I. Constant direction:

$$\theta = \text{const} = \text{atan}\left(\frac{h_b}{h_c}\right). \quad (17)$$

II. Varying direction:

$$\theta^{\alpha p} = \text{ varying } = \frac{1}{2}\left[\pi - \text{atan}\left(\frac{v_{j\neq}^{\alpha x}}{f_2/2}\right)\right], \quad (18)$$

where f_a(also presented as σ_c) = axial stresses = N/A_{col}, v_{jh}^{exp} = joint horizontal shear stress = $V_{jh}\,^{exp}/A_{col}$, N = axial load on the column, and A_{col} = X-area of column $= b_c \times h_c$

For the most typical uses of FRP sheets, a simple formula is available to determine the corresponding area of the FRP, $A_{f/nj}$ [69]. Afterward, the *Eqs. (16)-(18)* are derived to calculate the area of joined FRP sheets as follows:

I. Uniaxial fabric having fibers in the direction of the beam axis $(0°)$ or column axis $(90°)$:

$$\begin{cases} A_{f,M} = n_l \cdot n_s \cdot t_f \cdot h_b \cdot \sin\theta \text{ for } \beta = 0°, \\ A_{f,Q} = n_l \cdot n_s - t_f \cdot h_b \cdot \cos\theta \text{ for } \beta = 90°. \end{cases} \quad (19)$$

II. Bidirectional fabric having fibers in the direction of beam and column axes $(0°, 90°)$:

$$A_{f,\,m} = n_l \cdot n_s - t_f \cdot h_b \cdot \cos\theta - (1 + \tan^2\theta). \quad \textbf{(20)}$$

III. Quadriaxial fabric having any fibers in the direction of the beam $(0°)$ and column $(90°)$ axes and $\pm 45°$:

$$A_{f,M} = n_l \cdot n_s \cdot t_f \cdot h_b \cdot \cos\theta \cdot (1 + \tan\theta + 2\tan^2\theta). \quad \textbf{(21)}$$

Areas of FRP strips and sheets with fiber inclinations other than $0°, 45°$, and $90°$are determined using *Eqs. (19)-(21)*.

$$A_{f,m} = n_l \cdot n_s \cdot t_f \cdot b_f, \quad \textbf{(22)}$$

where n_s indicates if one or two faces have been reinforced with FRP for shear in the load plane of the joint panel, n_1 denotes the number of layers of FRP used on the strengthened side, n_1 represents the identical thickness of the FRP's dry fibers solely and denotes the width of the FRP sheet, calculated utilizing *Eq. (20)*, based on the angle of inclination of the fiber:

$$\begin{cases} b_f = h_b/\cos\beta & \text{for } \beta < \theta, \\ b_f = h_b/\sin\beta & \text{for } \beta \geq \theta. \end{cases} \quad \textbf{(23)}$$

Eq. (23) is then given for the FRP's discontinuous strips (partially wrapped with strips). To get b_j for the FRP's discontinuous strips (those only partly wrapped with strips), *Eq. (24)* is used.

$$\begin{cases} b_f = (w_f \cdot n_{str})^2 \cos\beta/h_b & \text{for} \quad \beta < \theta, \\ b_f = (w_f \cdot n_{str})^2 \sin\beta/h_c & \text{for} \quad \beta \geq \theta, \end{cases} \quad \textbf{(24)}$$

where w_j , n_{str} β are the width of each strip, the number of strips if the beam is partly wrapped with strips, and the angle at which the FRP fibers are oriented concerning the beam axis, respectively. The total surface area of all FRP sheets or stips (based on the inclination of the fibers) is computed independently. For an assembly, the total area of all FRP types is used to calculate the equivalent FRP area $A_{f,A}$.

3.2 | Analysis of Experimental Tests

To analyze the Strengthened RC T-Beam Performance in Combined Torsion and Shear, the numeric analysis indicates that the final torque of beam A2 is greater than that of beam A1, and the reference beam (AB) cracked earlier than the other beams. The maximum angle of twist, cracking torque, and final torque for the beams A1, A2, and AB are all listed in *Table 1*, along with experimental and numerical data. The use of FRP strips enhances the torsional capacity of RC beams, as shown by the comparison of experimental and numerical data. The section of the beam that is subjected to testing is situated between two load locations. As the load on the transverse steel grew, the strain was recorded. Strain, as seen in the graphs, is the lengthening of the transverse steel due to the applied load to these beams. When cracking occurred, it was preferable to use transversal steel, which could withstand a higher weight since the concrete could only support a smaller fraction of the load. However, there is a restriction on how much stress transversal steel can withstand before it begins to deform. Also, distinct behavior patterns emerge when FRPs are arranged and oriented in various ways. The numerical and experimental results are very similar, as shown in *Fig. 5*. Six factors have been found to affect significantly (V_{cf}), including the modulus of elasticity of FRP bar (E_f), CS (f'_c), flexural reinforcement ratio (ρ_f), shear span depth ratio (a/d), the width of the web (b_w) and effective depth (d). The input layer

could have only six neurons to use these six parameters primarily. Both shear strength (V_{cf}) and shear stress ($V_{cf}f(b_w d)$) are relevant here. *Fig. 6* shows the shear strength of FRP concrete in three specimens.

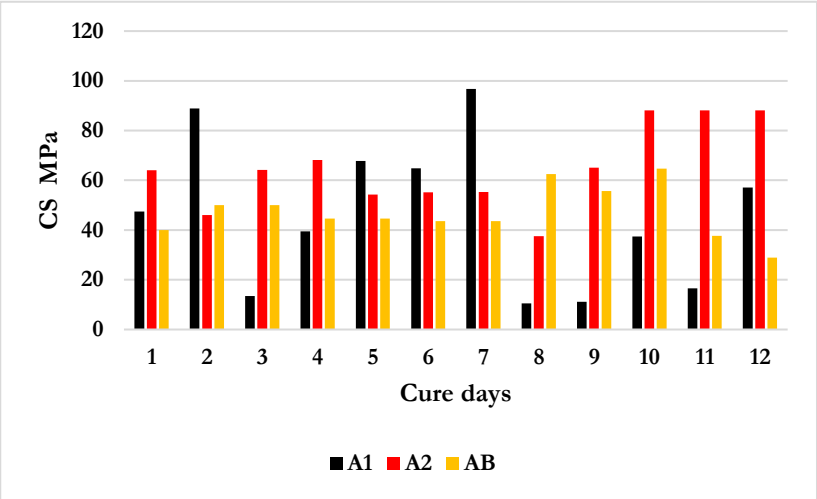

Fig. 5. CS of FRP concrete in three specimens.

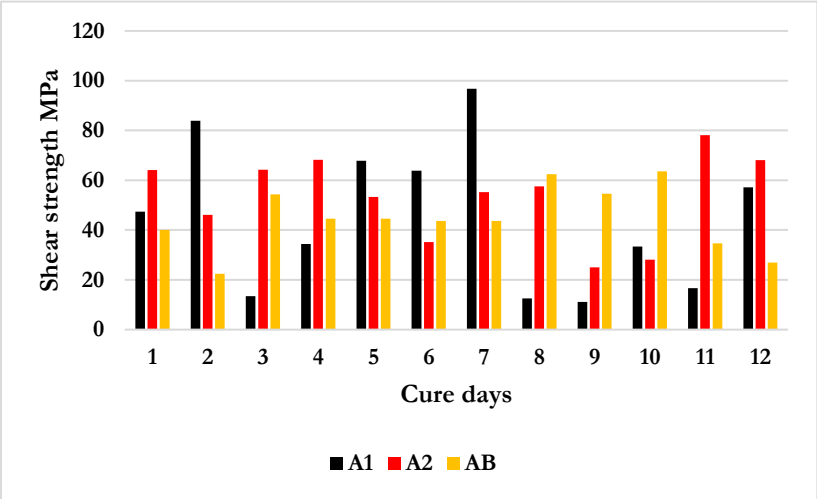

Fig. 6. Shear strength of FRP concrete in three specimens.

It's commonly accepted that there's a linear relevance between the shear strength and the width (b_w) of RC flexural members. Because of this, the ANN may be trained for the desired values of the normalized shear strength relative to the member width ($V_{cf} \mid b_w$) or shear stress ($V_{cf}(b_w d)$). The FRP full wrapping retrofitting method is more efficient than an extended FRP U-jacket. However, despite being the most practical option, the FRP U-jacket retrofitting technique has the lowest efficiency of the available schemes. The structural performance of the beam was enhanced by the extended FRP U-jacket, which allowed it to withstand more twists than the FRP U-jacket alone. Incorporating an FRP extension to the flange, which slows the spread of cracks in the flange, is responsible for the improvement. A full wrap in FRP is the best method for updating an older building. For the new beams, this method of retrofitting is preferable, as it allows for full wrapping of the sections.

On the other hand, it isn't easy to reach all sides of the present beams. As a result, it is not always simple to correctly implement the flange jacket for the FRP complete wrapping approach in real-world situations. The best ANN models for the given architecture were selected after training 288 different networks, and their RMSE values are proposed in *Table 3*. *Table 3* displays the mean of the following error metrics (μ), standard

deviation (σ), squared correlation coefficient (R^2), coefficient of variation (COV), and RMSE. *Fig. 7* is an example of a clustered column chart, where the x-axis shows the compared categories and the y-axis shows the values. Different information series are represented in separate columns, and comparisons for the same category are displayed by grouping the columns. Normal practice has the horizontal axis standing in for the various classes and the vertical axis representing the various numerical scores.

Table 3. Statistical parameters of (V_{exp}/V_{pred}) for ANN.

	Mean (V_{exp}/V_{pred})	SD	COV%	Minimum	Maximum	Range	RMSE	MAE	R^2
A1	1.811	0.416	22.06	1.14	3.75	2.62	30.5	24.3	0.576
A2	1.303	0.283	21.61	0.45	2.52	2.04	21.0	14.8	0.793
AB	1.092	0.225	20.83	0.45	1.84	1.36	21.5	11.8	0.784

A clustered column chart was used in this study to compare the data values A1, A2, and AB (*Fig. 7*). The columns, or "clustered," are grouped to show the relationship between the different values. The study's clustered column chart was designed to show the relationship between data values A1, A2, and AB and how they compare across categories. Categories being compared are shown on the x-axis of the chart, while values are represented on the y-axis. Each column in the chart represents a different data series, with A1, A2, and AB being the three series being compared. The chart effectively presents the data and easily compares the A1, A2, and AB values. A1 and A2 have similar values, while AB has a distinct value. It can also be observed that the values of A1 and A2 are close to each other and are higher than AB.

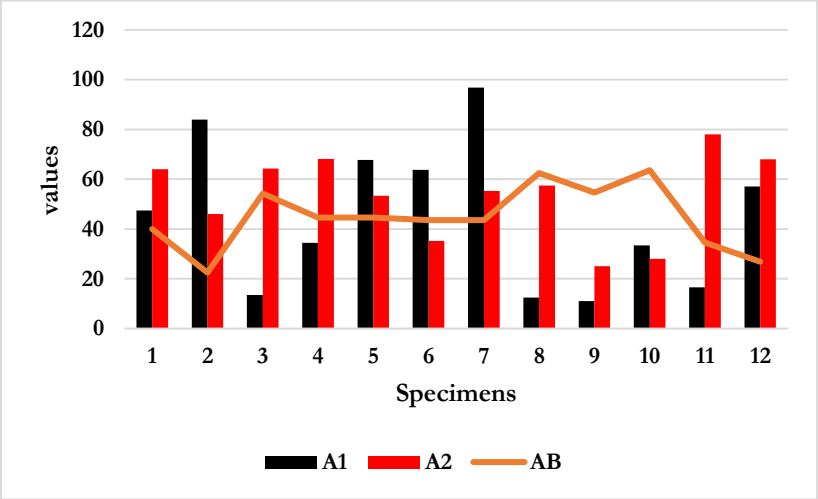

Fig. 7. The clustered plot of three samples.

3.3 | Results and Findings

In this research, two different effective depths, 180 mm (A1) and 400 mm (A2), were applied to test the shear strength of RC beams. Three different mixtures were made to limit the volume shifts of the concrete. Every concrete sample had the same water-to-binder ratio (W/B) and the same volumetric ratio of liquid (water, including the SRA) and aggregate contents. The beams were cast with the specified dimensions of height (200 mm for A1 and 600 mm for A2), width (200 mm for both A1 and A2), and effective depth (1500 mm for A1 and 4500 mm for A2). The specimens were cured for 28 days before testing. The outcomes of the study indicated that the average CS of the concrete was 30 ±1.5 MPa. The average shear solidity of the A1 beams was calculated as 8.56 ± 0.73 MPa, while the average shear solidity of the A2 beams was found to be 8.79 ± 0.58 MPa. These results indicate that the beams' effective depth significantly impacted the shear strength of the beams. The use of FRP strips as reinforcement was found to be an effective model for increasing the shear strength of the beams. The average shear solidity of the A1 beams reinforced with FRP strips was 12.48

± 0.99 MPa, while the average shear solidity of the A2 beams reinforced with FRP strips was 12.75 ± 0.82 MPa. These results indicate that using FRP strips as reinforcement raised the shear solidity of the beams by 46% and 44% for A1 and A2 beams, respectively. There is also a comparison between the findings of this work and the existing analytical methods and the prediction of the shear strength when considering ANN methods. The ANN forecasts were found to be in excellent agreement with the empirical findings. The impact of torsion on the shear strength of the beams is also declared in the study. The results indicated that torsion had a negative effect on the shear strength of the beams. The results of this study can be used to improve the design and placement methods of FRP composites in RC beams to increase their shear strength. The average shear strength of the A1 beams with torsion was 7.98 ± 0.68 MPa, while the average shear strength of the A2 beams with torsion was 8.13 ± 0.53 MPa. These results show that torsion reduced the shear strength of the beams by 7% and 8% for the A1 and A2 beams, respectively.

Beams shear reinforced using FRP in both U-jacketing and complete wrapping arrangements are represented in the database. The chosen experiments also demonstrate a wide range of beam geometry ratios, material attributes, reinforcement ratios, and failure loads. The experimental database includes data on the load configuration, beam geometry, mechanical characteristics, and arrangement of concrete and internal reinforcement, as well as the external reinforcement's geometry, configuration, and mechanical characteristics. Given the large number of elements that might affect the shear failure mode, it is crucial to carefully pick the input variables to get the best possible ANN configuration, and it is necessary to use the size of the training set to decide the number of input parameters. One of the most crucial aspects of making this method work is selecting input parameters that accurately reflect the features of the topic under investigation.

On the one hand, there must be a lot of parameters so that the system can be represented accurately. However, a huge number of input neurons in the ANN may limit its ability to learn effectively and accurately. In this scenario, the various design suggestions' shear capacity formulas were presented to facilitate the selection of the input values. One of the most crucial factors in determining the method's effectiveness is how the input parameters indicating the features of the topic under study are selected.

On the one hand, sufficient parameters must reflect the system accurately. On the other side, the training of the ANN may be hindered by an excessive number of input neurons. The shear capacity formulas of the various design proposals were summarized earlier, and these equations have served as a guide in selecting the appropriate input parameters here. That's why we could determine the theoretical shear capacity of the collected empirical beams using the four different designs. Fifteen theoretical predictions were made by appropriately combining the various FRP design guidelines with the various concrete codes. The results show that the most accurate predictions were made when FIP Bulletin 14's design guidelines were followed. ANN's input parameters were chosen using FIB Bulletin 14, EHE, and Eurocode 2 as a base, but this does not lead to the conclusion that this is the best guidance for FRP strengthening planning. *Fig. 8* shows a 3D surface plot that was generated to analyze the relationship between depth (d = mm), width (b_w = mm), and shear capacity (V_{cf}, in N) of a structural element. The plot shows the variation in shear capacity as the depth and width of the element change. It is seen that as the depth and width become higher, the shear capacity of the element also increases. However, it is crucial to remember that there can be a threshold of diminishing returns, after which increasing the depth and breadth may not significantly enhance the shear capacity. Additionally, it is important to consider other factors, such as material properties and boundary conditions, when interpreting the plot results (*Fig. 8*).

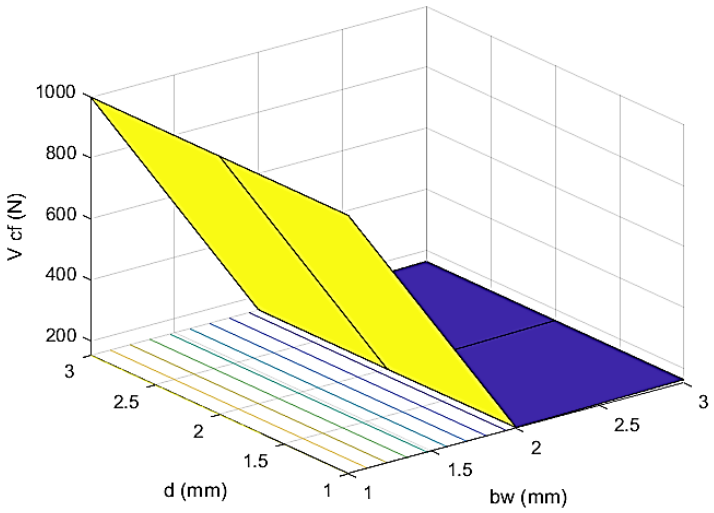

Fig. 8. Shear solidity of FRP-RC in the 3D surface plot.

In this study, the control group, AB, has specified dimensions of height (100mm), width (200mm), and effective depth (1000mm), which are different from the other two groups (A1 and A2) in terms of height, effective depth, and loading conditions. The control group also has a lower nominal load for shear failure (130 KN) and bending failure (300 KN) compared to the other groups (134 KN and 340 KN for A1, 280 KN, and 1000 KN for A2). The study will compare the shear strength and bending strength of the control group with the other groups to investigate the impact of the various dimensions and loading conditions on the strength of the beams. The study uses the results to improve FRP composites' design and placement methods in RC beams to increase their shear and bending strength. In this work, the shear strength of RC beams was considered by utilizing two effective depths of 180 mm (A1) and 400 mm (A2). The control group (AB) had a different dimension with a height of 100mm, width of 200mm, and effective depth of 1000 mm. The nominal loads for shear failure applied to AB, A1, and A2 were 130 KN, 134 KN, and 280 KN, respectively. The nominal load for bending failure applied to AB, A1, and A2 were 300 KN, 340 KN, and 1000 KN, respectively. The A1 and A2 beams had an average CS of 30 1.5 ± MPa and average shear strength of 8.56 ± 0.73 MPa and 8.79 ± 0.58 MPa, respectively. Using FRP strips as reinforcement raised the shear strength of the A1 beams by 46% and 44% for the A1 and A2 beams, respectively. The work also considered torsion's impact on the beams' shear strength. The findings indicated that torsion had a negative effect on the shear strength of the beams, reducing the shear strength by 7% and 8% for A1 and A2 beams, respectively. The control group (AB) had lower strength than A1 and A2. This is due to the difference in dimensions and the applied load. The results show that the effective depth of the beams had an important effect on the shear strength of the beams, and using FRP strips as reinforcement was a beneficial technique for increasing the shear strength of the beams. The results of this work can be used to enhance the design and placement methods of FRP composites in RC beams to increase their shear strength. In this research, the performance of ANN was evaluated to predict the shear strength of FRP RC. Three different ANN algorithms, A1, A2, and AB, were trained and tested using empirical information. The forecast results were compared to the corresponding empirical values, and several statistical measures were used to measure the efficiency of the ANN algorithms. The results demonstrate that the ANN model could forecast the shear strength of FRP RC with varying levels of accuracy. The mean of the ratio of empirical to forecasted values Mean (V_{exp}/V_{pred}) for A1, A2, and AB were 1.811, 1.303, and 1.092, respectively. The Standard Deviation (SD) of the A1, A2, and AB ratios were 0.416, 0.283, and 0.225, respectively, indicating that the predictions were generally near empirical values. The Coefficients of Variation (COV%) for A1, A2, and AB were 22.06, 21.61, and 20.83, respectively, indicating that the predictions were generally consistent with the experimental values. The last and highest ratio values for A1, A2, and AB were 1.14 and 3.75, 0.45 and 2.52, and 0.45 and 1.84, respectively, indicating that the predictions were generally within the range of the experimental values. The range of the

ratios for A1, A2, and AB were 2.62, 2.04, and 1.36, respectively, indicating that the predictions could generally capture the variation in the experimental values (*Table 3*). The Root Means Square Error (RMSE) and Mean Absolute Error (MAE) for A1, A2, and AB were 30.5 and 24.3, 21.0 and 14.08, and 21.5 and 11.8, respectively, indicating that the predictions were generally near the empirical values. The coefficient of determination (R^2) for A1, A2, and AB were 0.576, 0.793, and 0.784, respectively, indicating that the predictions could generally capture the variation in the experimental values. Finally, the outcomes of this study show that ANN can be an efficient tool for forecasting the shear strength of FRP RC. Among the three models, A2 and AB performed better in forecasting the shear strength of FRP RC. The findings also propose that the ANN models can be utilized as a reliable tool for forecasting the shear strength of FRP RC. Although, further study is needed to enhance the precision of the ANN model.

4 | Conclusion

This work has conducted the solidity of RC beams with FRP-enhanced shear. With the help of a database of experimental results, a neural network has been considered to make forecasts about this shear strength. To demonstrate the high precision of the solidity values acquired from ANN, a comparison study was conducted between the neural network predictions, the experimental results, and the forecasts of other design proposals. The shear span-to-depth rate, the external reinforcement arrangement, the elastic modulus of FRP in the primary fiber orientation, and the angle between the principal fiber orientation and the member's longitudinal axis are all important considerations. This work investigated the shear strength of RC beams applying two diverse, effective depths, 180 mm (A1), 400 mm (A2), and 600 mm (AB). Concrete volume fluctuations were regulated using three distinct mix proportions, maintaining a consistent w/c and volumetric ratio of liquid-to-aggregate contents. The findings of this research showed that one major factor with a significant impact on the shear strength of the beams is the effective depth of the beams, with the average shear solidity of the A1 beams being 8.56 ± 0.73 MPa and the average shear strength of the A2 beams being 8.79 ± 0.58 MPa. The use of FRP strips as reinforcement was proposed to be a beneficial method for increasing the shear strength of the beams. The average shear strength of the A1 beams reinforced with FRP strips was 12.48 ± 0.99 MPa, and the average shear strength of the A2 beams reinforced with FRP strips was 12.75 ± 0.82 MPa. This represents an enhancement in shear strength of 46% and 44% for A1 and A2 beams, respectively. The results of this work were also compared with the existing analytical methods and the forecast of the shear strength using ANN, and they were found to agree. The study also looked at the impact of torsion on the shear strength of the beams, and they displayed that the torsion had a negative effect on the shear strength of the beams. The average shear strength of the A1 beams with torsion was 7.98 ± 0.68 MPa, and that of the A2 beams with torsion was 8.13 ± 0.53 MPa. This represents a 7% and 8% reduction in shear strength for A1 and A2 beams, respectively. Finally, the results of this work can be used to improve the design and placement methods of FRP composites in RC beams to increase their shear strength. In general, this study provides valuable insights into the shear strength of RC beams and the use of FRP composites as reinforcement. In conclusion, the results of this study show that the ANN algorithms can be a useful method to forecast the shear strength of FRP-RC.

The ANN model, A1, A2, and AB, could forecast the shear strength with varying levels of accuracy. The A2 and AB models performed better in forecasting the shear strength of FRP RC, with a coefficient of determination (R^2) of 0.793 and 0.784, respectively. The results also suggest that the ANN models are reliable methods for predicting the shear strength of FRP RC. However, further study is needed to improve the accuracy of the prediction of the ANN model. The results show that the ANN model can be valuable in designing and analyzing FRP-RC structures. This study has a few limitations to consider when interpreting the results. One limitation is that the study used a limited number of experimental data, and the ANN models were trained and tested using the same dataset, which might affect the accuracy of the results.

Additionally, the study only considered a specific type of FRP-RC, and the results may not directly apply to other types of RC or other materials. Furthermore, the study did not consider other factors that may affect

the shear strength of FRP-RC, such as the type of FRP, the bond between the FRP and concrete, and the thickness of the FRP. Further research is needed to investigate these factors and enhance the forecast accuracy of the ANN models.

Author Contributions

The authors contributed equally to this work.

Funding

The authors declare that this research did not receive any specific grant from public, commercial, or not-for-profit funding agencies.

Data Availability

The data used in this study are available upon request from the corresponding author.

Conflict of Interest

The authors declare no conflict of interest regarding the publication of this manuscript.

References

[1] Kani, G. N. J. (1966). Basic facts concerning shear failure. *ACI journal proceedings, 63*, 675-692. DOI: 10.14359/7644

[2] ACI Committee. (2008). *Building code requirements for structural concrete (ACI 318-08) and commentary*. https://www.concrete.org/Portals/0/Files/PDF/Previews/318-08_preview.pdf

[3] Code, P. (2005). *Eurocode 2: design of concrete structures-part 1--1: general rules and rules for buildings* (Vol. 668). https://www.saiglobal.com/PDFTemp/Previews/OSH/IS/EN/2005/I.S.EN1992-1-1-2005.pdf

[4] Elsanadedy, H. M., Abbas, H., Al-Salloum, Y. A., & Almusallam, T. H. (2016). Shear strength prediction of HSC slender beams without web reinforcement. *Materials and structures/materiaux et constructions*, *49*(9), 3749–3772. DOI:10.1617/s11527-015-0752-x

[5] Lee, J. Y., & Kim, U. Y. (2008). Effect of longitudinal tensile reinforcement ratio and shear span-depth ratio on minimum shear reinforcement in beams. *ACI structural journal*, *105*(2), 134–144. DOI:10.14359/19728

[6] Syroka-Korol, E., & Tejchman, J. (2014). Experimental investigations of size effect in reinforced concrete beams failing by shear. *Engineering structures*, *58*, 63–78. DOI:10.1016/j.engstruct.2013.10.012

[7] Lee, J. Y., Choi, I. J., & Kim, S. W. (2011). Shear behavior of reinforced concrete beams with high-strength stirrups. *ACI structural journal*, *108*(5). https://www.researchgate.net/profile/Sang-Woo-Kim-6/publication/268031194_Shear_Behavior_of_Reinforced_Concrete_Beams_with_High-Strength_Stirrups/links/56a6caa708ae997e22ba4eec/Shear-Behavior-of-Reinforced-Concrete-Beams-with-High-Strength-Stirrups.pdf

[8] Shariati, M., Davoodnabi, S. M., Toghroli, A., Kong, Z., & Shariati, A. (2021). Hybridization of metaheuristic algorithms with adaptive neuro-fuzzy inference system to predict load-slip behavior of angle shear connectors at elevated temperatures. *Composite structures*, *278*, 114524. DOI:10.1016/j.compstruct.2021.114524

[9] Davoodnabi, S. M., Mirhosseini, S. M., & Shariati, M. (2021). Analyzing shear strength of steel-concrete composite beam with angle connectors at elevated temperature using finite element method. *Steel and composite structures*, *40*(6), 853–868. DOI:10.12989/scs.2021.40.6.853

[10] Nouri, K., Sulong, N. H. R., Ibrahim, Z., & Shariati, M. (2021). Behaviour of novel stiffened angle shear connectors at ambient and elevated temperatures. *Advanced steel construction*, *17*(1), 28–38. DOI:10.18057/IJASC.2021.17.1.4

[11] Shariati, M., Mafipour, M. S., Mehrabi, P., Shariati, A., Toghroli, A., Trung, N. T., & Salih, M. N. A. (2021). A novel approach to predict shear strength of tilted angle connectors using artificial intelligence techniques. *Engineering with computers*, *37*(3), 2089–2109. DOI:10.1007/s00366-019-00930-x

[12] Naghipour, M., Niak, K. M., Shariati, M., & Toghroli, A. (2020). Effect of progressive shear punch of a foundation on a reinforced concrete building behavior. *Steel and composite structures*, *35*(2), 279–294. DOI:10.12989/scs.2020.35.2.279

[13] Shariati, M., Tahmasbi, F., Mehrabi, P., Bahadori, A., & Toghroli, A. (2020). Monotonic behavior of C and L shaped angle shear connectors within steel-concrete composite beams: An experimental investigation. *Steel and composite structures*, *35*(2), 237–247. DOI:10.12989/scs.2020.35.2.237

[14] Davoodnabi, S. M., Mirhosseini, S. M., & Shariati, M. (2019). Behavior of steel-concrete composite beam using angle shear connectors at fire condition. *Steel and composite structures*, *30*(2), 141–147. DOI:10.12989/scs.2019.30.2.141

[15] Mansouri, I., Shariati, M., Safa, M., Ibrahim, Z., Tahir, M. M., & Petković, D. (2020). Retraction note to: analysis of influential factors for predicting the shear strength of a V-shaped angle shear connector in composite beams using an adaptive neuro-fuzzy technique. *Journal of intelligent manufacturing*, *31*(1), 267. DOI:10.1007/s10845-019-01493-w

[16] Hosseinpour, E., Baharom, S., Badaruzzaman, W. H. W., Shariati, M., & Jalali, A. (2018). Direct shear behavior of concrete filled hollow steel tube shear connector for slim-floor steel beams. *Steel and composite structures*, *26*(4), 485–499. DOI:10.12989/scs.2018.26.4.485

[17] Paknahad, M., Shariati, M., Sedghi, Y., Bazzaz, M., & Khorami, M. (2018). Shear capacity equation for channel shear connectors in steel-concrete composite beams. *Steel and composite structures*, *28*(4), 483–494. DOI:10.12989/scs.2018.28.4.483

[18] Khanouki, M. M. A., Ramli Sulong, N. H., Shariati, M., & Tahir, M. M. (2016). Investigation of through beam connection to concrete filled circular steel tube (CFCST) column. *Journal of constructional steel research*, *121*, 144–162. DOI:10.1016/j.jcsr.2016.01.002

[19] Alam, M. S., & Hussein, A. (2013). Size effect on shear strength of FRP reinforced concrete beams without stirrups. *Journal of composites for construction*, *17*(4), 507–516.

[20] Yost, J. R., Gross, S. P., & Dinehart, D. W. (2001). Shear strength of normal strength concrete beams reinforced with deformed GFRP bars. *Journal of composites for construction*, *5*(4), 268–275.

[21] Razaqpur, A. G., Isgor, B. O., Greenaway, S., & Selley, A. (2004). Concrete contribution to the shear resistance of fiber reinforced polymer reinforced concrete members. *Journal of composites for construction*, *8*(5), 452–460. DOI:10.1061/(asce)1090-0268(2004)8:5(452)

[22] Nehdi, M., El Chabib, H., & Saïd, A. A. (2007). Proposed shear design equations for FRP-Reinforced concrete beams based on genetic algorithms approach. *Journal of materials in civil engineering*, *19*(12), 1033–1042. DOI:10.1061/(asce)0899-1561(2007)19:12(1033)

[23] ASCE-ACI Committee 445 on Shear and Torsion. (1998). Recent approaches to shear design of structural concrete. *Journal of structural engineering*, *124*(12), 1375-1417.

[24] Park, R., & Paulay, T. (1991). *Reinforced concrete structures*. John Wiley & Sons.

[25] Mohammadhassani, M., Nezamabadi-pour, H., Suhatril, M., & Shariati, M. (2014). An evolutionary fuzzy modelling approach and comparison of different methods for shear strength prediction of high-strength concrete beams without stirrups. *Smart structures and systems*, *14*(5), 785–809. DOI:10.12989/sss.2014.14.5.785

[26] Shariati, M. (2013). *Behaviour of C-shaped shear connectors in stell concrete composite beams* (Doctoral Dissertation, Jabatan Kejuruteraan Awam, Fakulti Kejuruteraan, Universiti Malaya). https://koreascience.kr/article/JAKO202117457480171.pdf

[27] Shariati, A., Sulong, N. H., Suhatril, M., & Shariati, M. (2012). Investigation of channel shear connectors for composite concrete and steel T-beam. *International journal of the physical sciences*, *7*(11), 1828–1831.

[28] Shariati, M., Ramli Sulong, N. H., & Arabnejad Khanouki, M. M. (2010). Experimental and analytical study on channel shear connectors in light weight aggregate concrete. *Proceedings of the 4th international conference on steel composite structures* (pp. 21–23). Research Publishing Services.

[29] Shariati, M., Ramlisulong, N. H., Sinaei, H., Arabnejad Kh., M. M., & Shafigh, P. (2011). Behavior of channel shear connectors in normal and light weight aggregate concrete (experimental and analytical study). *Advanced materials research*, *168/170*, 2303–2307. DOI:10.4028/www.scientific.net/AMR.168-170.2303

[30] Mohammadhassani, M., Nezamabadi-Pour, H., Suhatril, M., & Shariati, M. (2013). Identification of a suitable ANN architecture in predicting strain in tie section of concrete deep beams. *Structural engineering and mechanics*, *46*(6), 853–868. DOI:10.12989/sem.2013.46.6.853

[31] Toghroli, A., Mohammadhassani, M., Suhatril, M., Shariati, M., & Ibrahim, Z. (2014). Prediction of shear capacity of channel shear connectors using the ANFIS model. *Steel and composite structures*, *17*(5), 623–639. DOI:10.12989/scs.2014.17.5.623

[32] Kara, I. F. (2011). Prediction of shear strength of FRP-reinforced concrete beams without stirrups based on genetic programming. *Advances in engineering software*, *42*(6), 295–304. DOI:10.1016/j.advengsoft.2011.02.002

[33] Bashir, R., & Ashour, A. (2012). Neural network modelling for shear strength of concrete members reinforced with FRP bars. *Composites part B: engineering*, *43*(8), 3198–3207. DOI:10.1016/j.compositesb.2012.04.011

[34] Nasrollahzadeh, K., & Basiri, M. M. (2014). Prediction of shear strength of FRP reinforced concrete beams using fuzzy inference system. *Expert systems with applications*, *41*(4/1), 1006–1020. DOI:10.1016/j.eswa.2013.07.045

[35] Lee, S., & Lee, C. (2014). Prediction of shear strength of FRP-reinforced concrete flexural members without stirrups using artificial neural networks. *Engineering structures*, *61*, 99–112. DOI:10.1016/j.engstruct.2014.01.001

[36] Golafshani, E. M., & Ashour, A. (2016). A feasibility study of BBP for predicting shear capacity of FRP reinforced concrete beams without stirrups. *Advances in engineering software*, *97*, 29–39. DOI:10.1016/j.advengsoft.2016.02.007

[37] Aiello, M. A., Ascione, L., Baratta, A., Bastianini, F., Battista, U., & Benedetti, A. (2014). *Guide for the design and construction of externally bonded FRP systems for strengthening existing structures*. https://hdl.handle.net/11311/883756

[38] Pansuk, W., & Sato, Y. (2007). Shear mechanism of reinforced concrete T-Beams with stirrups. *Journal of advanced concrete technology*, *5*(3), 395–408. DOI:10.3151/jact.5.395

[39] Foster, R. M., Brindley, M., Lees, J. M., Ibell, T. J., Morley, C. T., Darby, A. P., & Evernden, M. C. (2017). Experimental investigation of reinforced concrete t-beams strengthened in shear with externally bonded CFRP sheets. *Journal of composites for construction*, *21*(2), 4016086. DOI:10.1061/(asce)cc.1943-5614.0000743

[40] Ameli, M., Ronagh, H. R., & Dux, P. F. (2007). Behavior of FRP strengthened reinforced concrete beams under torsion. *Journal of composites for construction*, *11*(2), 192–200.

[41] Chalioris, C. E. (2007). Tests and analysis of reinforced concrete beams under torsion retrofitted with FRP strips. *WIT transactions on modelling and simulation*, *46*, 633–642. DOI:10.2495/CMEM070631

[42] Mohammadizadeh, M. R., & Fadaee, M. J. (2010). Experimental investigation on torsional strengthening of high-strength concrete beams using CFRP sheets. *Kuwait journal of science and engineering*, *37*(1B), 1–19.

[43] Hii, A. K. Y., & Al-Mahaidi, R. (2006). Experimental investigation on torsional behavior of solid and box-section RC beams strengthened with CFRP using photogrammetry. *Journal of composites for construction*, *10*(4), 321–329. DOI:10.1061/(asce)1090-0268(2006)10:4(321)

[44] Jing, M., Raongjant, W., & Li, Z. (2007). Torsional strengthening of reinforced concrete box beams using carbon fiber reinforced polymer. *Composite structures*, *78*(2), 264–270. DOI:10.1016/j.compstruct.2005.10.017

[45] Chalioris, C. E. (2008). Torsional strengthening of rectangular and flanged beams using carbon fibre-reinforced-polymers - Experimental study. *Construction and building materials*, *22*(1), 21–29. DOI:10.1016/j.conbuildmat.2006.09.003

[46] Deifalla, A., & Ghobarah, A. (2010). Strengthening RC T-Beams subjected to combined torsion and shear using FRP fabrics: experimental study. *Journal of composites for construction*, *14*(3), 301–311. DOI:10.1061/(asce)cc.1943-5614.0000091

[47] Triantafillou, T., Matthys, S., Audenaert, K., Balázs, G., Blaschko, M., & Blontrock, H. (2001). *Externally bonded FRP reinforcement for RC structures*. International Federation for Structural Concrete.

[48] Hii, A. K. Y., & Al-Mahaidi, R. (2006). An experimental and numerical investigation on torsional strengthening of solid and box-section RC beams using CFRP laminates. *Composite structures*, *75*(1–4), 213–221. DOI:10.1016/j.compstruct.2006.04.050

[49] Bernardo, L., & Taborda, C. (2020). Softened truss model for reinforced concrete beams under torsion combined with axial force. *Applied mechanics*, *1*(1), 79–96. DOI:10.3390/applmech1010006

[50] Protchenko, K., & Szmigiera, E. (2020). Post-Fire characteristics of concrete beams reinforced with hybrid FRP bars. *Materials*, *13*(5), 1248. DOI:10.3390/ma13051248

[51] Salih, R., Zhou, F., Abbas, N., & Mastoi, A. K. (2020). Experimental investigation of reinforced concrete beam with openings strengthened using frp sheets under cyclic load. *Materials*, *13*(14), 3127. DOI:10.3390/ma13143127

[52] Pohoryles, D. A., Melo, J., & Rossetto, T. (2021). Combined flexural and shear strengthening of RC T-beams with frp and TRM: Experimental study and parametric finite element analyses. *Buildings*, *11*(11), 520. DOI:10.3390/buildings11110520

[53] Abdolrasol, M. G. M., Suhail Hussain, S. M., Ustun, T. S., Sarker, M. R., Hannan, M. A., Mohamed, R., … Milad, A. (2021). Artificial neural networks based optimization techniques: A review. *Electronics (Switzerland)*, *10*(21), 2689. DOI:10.3390/electronics10212689

[54] Milad, A., Hussein, S. H., Khekan, A. R., Rashid, M., Al-Msari, H., & Tran, T. H. (2022). Development of ensemble machine learning approaches for designing fiber-reinforced polymer composite strain prediction model. *Engineering with computers*, *38*(4), 3625–3637. DOI:10.1007/s00366-021-01398-4

[55] Amani, J., & Moeini, R. (2012). Prediction of shear strength of reinforced concrete beams using adaptive neuro-fuzzy inference system and artificial neural network. *Scientia Iranica*, *19*(2), 242–248. DOI:10.1016/j.scient.2012.02.009

[56] Wang, J., Zou, X., & Feng, Y. (2015). Bilinear load-deflection model of fiber-reinforced polymer-concrete composite beam with interface slip. *Advances in mechanical engineering*, *7*(7), 1–14. DOI:10.1177/1687814015590312

[57] ACI Committee 440. (2002). *Guide for the design and construction of structural concrete reinforced with FRP Bars* (Vol. 88). https://basalt-fibers.com/wp-content/uploads/2021/05/Standart_ACI-4401R15.pdf

[58] IStructE. (1999). *Interim guidance on the design of reinforced concrete structures using fibre composite reinforcement*. Institution of Structural Engineers. https://www.thenbs.com/PublicationIndex/documents/details?Pub=IStructE&DocId=247901

[59] Mufti, A. A., & ISIS Canada. (2001). *Reinforcing concrete structures with fibre reinforced polymers*. ISIS Canada.

[60] Recommendations, J. (2006). Japan society of civil engineers (JSCE): recommendations for design and construction of ultra-high strength fiber-reinforced conerete Structures. *JSCE guidelines for concrete*, (9). https://www.jsce.or.jp/committee/concrete/e/hpfrcc_JSCE.pdf

[61] Michaluk, C. R., Rizkalla, S. H., Tadros, G., & Benmokrane, B. (1998). Flexural behavior of one-way concrete slabs reinforced by fiber reinforced plastic reinforcements. *ACI structural journal*, *95*(3), 353–365. DOI:10.14359/552

[62] Deitz, D. H., Harik, I. E., & Gesund, H. (1999). One-way slabs reinforced with glass fiber reinforced polymer reinforcing bars. *Special Publication*, *188*, 279-286. DOI:10.14359/5629

[63] Tureyen, A. K., & Frosch, R. J. (2003). Concrete shear strength: Another perspective. *Structural journal*, *100*(5), 609–615.

[64] El-Sayed, A. K., El-Salakawy, E. F., & Benmokrane, B. (2006). Shear strength of FRP-reinforced concrete beams without transverse reinforcement. *ACI materials journal*, *103*(2), 235-243.

[65] Diamantis, Z. G., Efthimeros, G. A., Photeinos, D. I., Tsahalis, D. T., Networks, A. N., & Passenger, V. (2001). Development of an artificial neural network (ANN) based virtual passenger. *4th European conference on noise control* (pp. 14–17). EURONOISE.

[66] Del Vecchio, C., Di Ludovico, M., Balsamo, A., Prota, A., Manfredi, G., & Dolce, M. (2014). Experimental investigation of exterior RC beam-column joints retrofitted with FRP Systems. *Journal of composites for construction*, *18*(4), 4014002. DOI:10.1061/(asce)cc.1943-5614.0000459

[67] Paulay, T., & Priestley, M. J. N. (1992). *Seismic design of reinforced concrete and masonry buildings* (Vol. 768). Wiley New York.

[68] Bousselham, A. (2010). State of research on seismic retrofit of RC beam-column joints with externally bonded FRP. *Journal of composites for construction*, *14*(1), 49–61.

[69] Del Vecchio, C., Di Ludovico, M., Prota, A., & Manfredi, G. (2015). Analytical model and design approach for FRP strengthening of non-conforming RC corner beam-column joints. *Engineering structures*, *87*, 8–20. DOI:10.1016/j.engstruct.2015.01.013